Optical and Quantum Electronics (2020) 52:8
https://doi.org/10.1007/s11082-019-2125-0

Photonic crystal fiber for robust orbital angular momentum transmission: design and investigation

Md. Mehedi Hassan[1] · Md. Anowar Kabir[1] · Md. Nadim Hossain[1] · Bipul Biswas[1] · Bikash Kumar Paul[1,2,3] · Kawsar Ahmed[1,2]

Received: 6 August 2019 / Accepted: 21 November 2019 / Published online: 28 November 2019

Abstract
In this paper, a novel design, photonic crystal fiber (PCF) has been reported to support more orbital angular momentum (OAM) modes for the first time. The cladding region formed by employing the three-layer chain shaped air cavities. The OAM properties and parameters are calculated by optimizing the design of the PCF. The simulation results can support 26 OAM modes with a wider bandwidth (750 nm). The confinement loss of the most OAM modes is below average 10^{-7} dB/m and the nonlinear coefficient is less than 4 W^{-1}/km. Some OAM modes with comparatively flat dispersion variation (such as 3.8684 ps/km-nm) for $HE_{2,1}$ are noticed from the design. Moreover, fundamental optical characteristics have been rigorously computed by utilizing the finite element method. Now, it can be anticipated that, these excellent optical characteristics confirm the introduced design as a prominent candidate for the OAM transmission and other relevant areas of optical communications.

Keywords Orbital angular momentum (OAM) · Photonic crystal fiber (PCF) · Mode division multiplexing (MDM) · Space division multiplexing (SDM)

1 Introduction

The orbital angular momentum (OAM) is the recently used consolidated multiplexing process concerning light for securing information. It is also a space division multiplexing (SDM) technology that is used in free space for optical communication (Huang et al. 2014). For the optical transmissions, the OAM introduced with vacuum communication (Brunet et al. 2014). Nowadays, optical communication confronts different types of

✉ Kawsar Ahmed
k.ahmed.bd@ieee.org; kawsar.ict@mbstu.ac.bd; kawsarit08050@gmail.com

[1] Department of Information and Communication Technology, Mawlana Bhashani Science and Technology University, Santosh, Tangail 1902, Bangladesh

[2] Group of Bio-photomatix, Mawlana Bhashani Science and Technology University, Santosh, Tangail 1902, Bangladesh

[3] Department of Software Engineering, Daffodil International University, Sukrabad, Dhanmondi, Dhaka 1207, Bangladesh

challenges such as the transmission of big data, telecommunication, broadcast, community antenna television coaxial cable (CATV), high-definition television (HDTV) for medium blocking and insufficient capacity of data transmission. Recently, for multimode fiber, the SDM technology provides the OAM method that enhances the capacity and efficiency of optical communication (Zhang et al. 2018; Richardson et al. 2013; Zhu et al. 2016; Li et al. 2018).

The beams of OAM individualized by $e^{(il\varphi)}$ (Chen et al. 2016), where the topological charge is expressed by l and it is an integer number (…., −3, −2, −1, 0, +1, +2, +3,….) and azimuthal angle is expressed by φ. The azimuthal angle (φ) of a point in cylindrical or spherical coordinates is the positive angle between the projection of the vector to the XY-plane and positive X-axis (Zhu et al. 2016; Allen et al. 1992). Every positive (+) and negative (−) topological charges are spatially orthogonal to each and another (Jiao et al. 2019). There are several methods to achieve an OAM beam like twisted fiber (Wong et al. 2012), helical lattice (Fang and Wang 2015), etc. There are various applications such as optical communication (Wang et al. 2012), particle trapping (Padgett and Bowman 2011), high-resolution imaging (Tamburini et al. 2006) and many more (Heng et al. 2017) of the OAM beams.

For improving the number of modes, Liu et al. (2019a) designed a dual-cladding photonic quasi-crystal fiber with 6 OAM modes for the OAM optical communication system. The quasi-periodic structure used in the photonic quasi-crystal fiber (Liu et al. 2019b, c; Li et al. 2019) such as sensing (Shi et al. 2019; Liu et al. 2019d), filters (Liu et al. 2018; Yan et al. 2018), nanocavity (Ren et al. 2018), metasurface (Tang et al. 2019), lens (Liu and Fan 2018), etc. Zhang et al. (2015) proposed a C-PCF with silica as the background material supporting 10 OAM modes to transmit in one fiber. A hollow-core fiber was proposed by Li et al. (2016) that supports 16 OAM modes with high confinement loss. A C-PCF proposed by Hu et al. (2016) that supports 26 OAM modes with As_2S_3 as background material. Wang et al. (2018) is also designed a PCF with 26 OAM modes. Xu et al. (2017) proposed a C-PCF supporting 30 OAM modes with negative dispersion. The proposed PCF of Lei et al. (2018) supports more OAM modes (76 OAM modes). But that was not enough for stable transmission. So, there is still room to design a novel PCF with larger OAM modes based on PCF with better output.

The high number of OAM mode is good for the encoding of data transmission. The same number of the OAM mode is useful for detecting receiving information with respect to sending information. When the sender sends data to the receiver, then it has to find out the similarities between sending and receiving data. By checking the mode properties of two transmission sides, the receiver ensures require data which transmit by the sender. In the OAM modulation process, the sender sends a carrier signal with the message signal; where the carrier signal carries the OAM mode properties. So, the OAM mode plays an important act in optical communication. The traditional optical fiber fails to transmit the OAM mode thus we have to design a special PCF for supporting multimode and also to achieve good parameters of a fiber. The difference between the two adjacent effective refractive indexes of the OAM *HE* and *EH* modes must be greater than 10^{-4} ($\Delta n_{eff} > 10^{-4}$) (Zhang et al. 2017a). The OAM transmission is supported by many unique PCF like spiral PCF (Nandam and Shin 2018), C-PCF with a square hole (Bai et al. 2018), dual guided ring-core PCF (Xu et al. 2018), C-PCF (Zhang et al. 2018). These are separately good for confinement loss, dispersion, nonlinearity, and numerical aperture, but not better for the robust transmission.

This paper proposed a chain shaped photonic crystal fiber that is composed of the three well-structured chain type air holes ring with a large air hole and the background material is composed of fused silica. This structure of PCF is novel for OAM transmission. This novel design of PCF supports 26 modes with 750 nm bandwidth. This PCF supports a low dispersion variation of 3.8684 ps/km-nm for the $HE_{2,1}$ mode, and 5.1421 ps/km-nm for the $TE_{0,1}$ mode with low confinement loss that is 3.19×10^{-10} dB/m at wavelength 1.80 µm.

2 Model and algorithm

As mention before, the proposed three-layer chain shaped air holes with a hollow-core C-PCF is designed and simulated by COMSOL Multiphysics 4.3b software. The hollow-core PCF is the part of PCFs that guide light through the core (Monfared 2018). The three well-patterned circular ring type chain shaped air holes would decrease the light outpouring of optical fiber. The radius of the core of the proposed model is 3.7 µm. The large core increases the number of OAM modes (Zhang et al. 2017a). The air holes are made by the Bezier Polygons. Seven Cartesian points are needed to build this type of curve. The width of each polygon is 1.5 µm ($w_2=w_3=w_4=1.5$ µm) and each co-ordinate has two levels that are totally eight levels. The area between the outer circle and the inner circle is called PML (Perfectly Matched Layer) and the width between them (w_1) is also 1.5 µm. It is added here to truncate unwanted nonphysical scattering. All the numerical analysis are implemented by using the PML and the FEM. And the background material is fused silica with a refractive index of 1.446 (Monfared et al. 2013). The refractive index (RI) is calculated by the Sellmeier Eq. (1) (Biswas et al. 2019).

$$\mathrm{n}(\lambda) = \sqrt{1 + \sum_{i=1}^{m} \frac{A_i \lambda^2}{\lambda^2 - \lambda_i^2}} \tag{1}$$

where m,λ_i^2 and A_i are the Sellmeier coefficients and n(λ) represents the RI that varies with wavelength. The cladding of the proposed PCF is constructed by fused silica. For fused silica, $m=3$. The complete design of the PCF is shown in Fig. 1.

The OAM modes in the PCF can be expressed by the combinations of even and odd modes of *EH* and *HE*. It can be defined by Eqs. (2) and (3) (Pakarzadeh and Sharif 2019; Zhang et al. 2017b).

$$\left\{ \begin{array}{l} OAM^{\pm}_{\pm l,m} = HE^{even}_{l+1,m} \pm jHE^{odd}_{l+1,m} \\ OAM^{\mp}_{\pm l,m} = EH^{even}_{l-1,m} \pm jEH^{odd}_{l-1,m} \end{array} \right\}; \quad (1 > 1) \tag{2}$$

$$\left\{ \begin{array}{l} OAM^{\pm}_{\pm 1,m} = HE^{even}_{2,m} \pm jHE^{odd}_{2,m} \\ OAM^{\mp}_{\pm 1,m} = TM_{0,m} \pm jTE_{0,m} \end{array} \right\}; \quad (l = 1) \tag{3}$$

where HE and EH are the composite mode of the OAM beam. The two main types of each mode are even and odd that obtains after π/2 phase difference of the modes. The sign of "±l" defines the right or left wave front orbit direction. Where l is a topological charge, j denotes a π/2 phase shift, and m denotes the radial order for the OAM mode, and equal to 1. The OAM mode does not support m > 1 because it causes "accidental degeneracies" (Pakarzadeh and Sharif 2019). Because it is a problem for the encoding, multiplexing and demultiplexing of the OAM modes. So, we use a lower-order radial mode (m = 1) (Zhang et al. 2018).

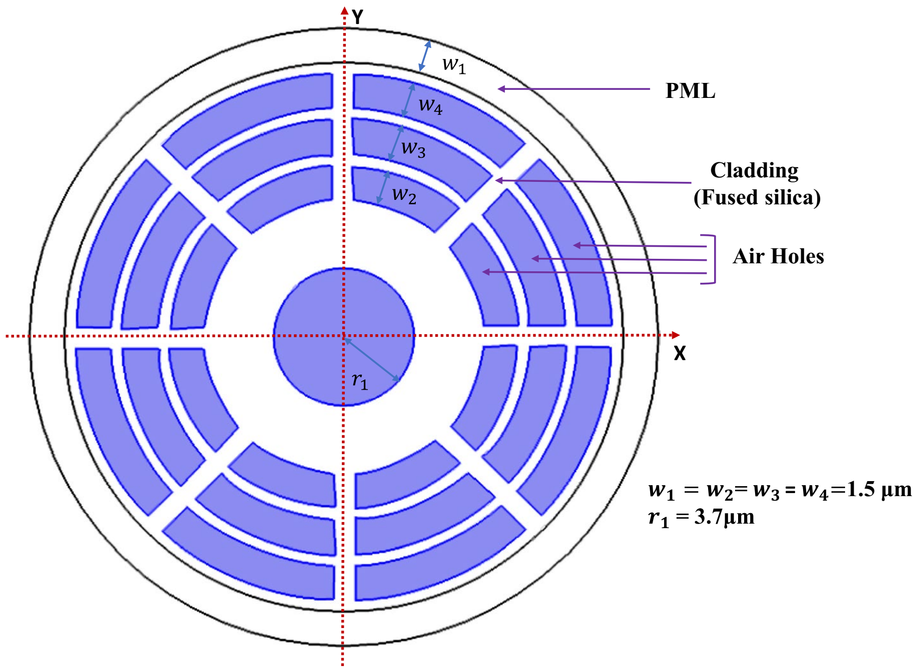

Fig. 1 The cross-section view of the proposed PCF

By applying the Eqs. (2) and (3), the proposed structure is supported 26 modes, these are $OAM^{\pm}_{\pm 1,1}\{HE_{2,1}\}, OAM^{\pm}_{\pm 2,1}\{HE_{3,1}, EH_{1,1}\}, OAM^{\pm}_{\pm 3,1}\{HE_{4,1}, EH_{2,1}\}, OAM^{\pm}_{\pm 4,1}\{HE_{5,1}, EH_{3,1}\}, OAM^{\pm}_{\pm 5,1}\{HE_{6,1}, EH_{4,1}\}, OAM^{\pm}_{\pm 6,1}\{HE_{7,1}, EH_{5,1}\}, OAM^{\pm}_{\pm 7,1}\{HE_{8,1}, EH_{6,1}\}$.

The proposed PCF is supported by all the selected modes from the wavelength the ranges from 1.2 to 1.95 µm and simulations are done by those modes. It also supports some eigenmodes such as $TE_{0,1}$ and $TM_{0,1}$, but they can't combine. Because the propagation constants of $TE_{0,1}$ and $TM_{0,1}$ modes are different.

The quality of the OAM based PCF depends on more numbers of the OAM modes. Because, it increases the capacity of transmission and also ensures the robust transmission. The encoding and multiplexing of lights are developed by the good quality of OAM mode. Therefore, the light intensity imbricate factor to qualitatively calculate the mode quality through the Eq. (4) (Zhang et al. 2017b).

$$\eta = \frac{I_r}{I_c} = \frac{\iint_{rings} \left|\vec{E}\right|^2 dxdy}{\iint_{cross-section} \left|\vec{E}\right|^2 dxdy} \tag{4}$$

where I_r defines the normal mode concentration of the ring area where all the OAM modes will be confined and I_c denotes the average mode intensity in full exploded view area of the C-PCF. In Fig. 2, different OAM mode intensity order of eigenmodes and the wave front phase are exhibited.

For all modes, proposed PCF gains flat dispersion, less nonlinearity, better numerical aperture, less confinement loss and other OAM properties.

Dispersion is evaluated by Eq. (5) (Zhang et al. 2018).

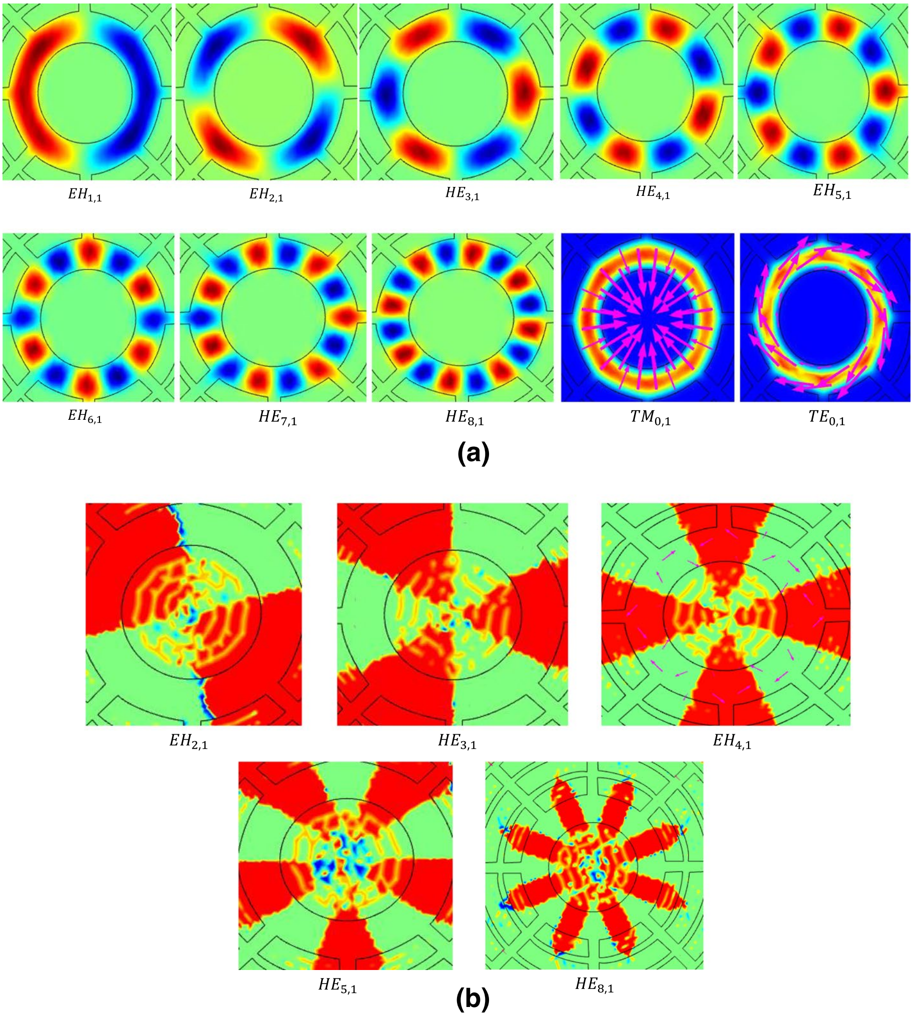

Fig. 2 **a** The intensity ordinations of $EH_{1,1}$, $EH_{2,1}$, $HE_{3,1}$, $HE_{4,1}$, $EH_{5,1}$, $EH_{6,1}$, $HE_{7,1}$, $HE_{8,1}$, $TE_{0,1}$ and $TM_{0,1}$ modes, **b** the phase ordinations of $EH_{2,1}HE_{3,1}$, $EH_{4,1}$, $HE_{5,1}$ and $HE_{8,1}$ modes

$$D = -\frac{\lambda}{c}\frac{d^2 Re\left[n_{eff}\right]}{d\lambda^2} \quad (5)$$

where $Re\left[n_{eff}\right]$ denotes the real values of the effective refractive index and c defines the velocity of light in the vacuum.

The differences of the refractive index can be evaluated through Eq. (6) (Pakarzadeh and Sharif 2019). This difference is performed on two adjacent vector mode.

$$\Delta n_{eff} = \left| n_{eff_{HE_{l+1,m}}} - n_{eff_{EH_{l-1,m}}} \right| > 10^{-4} \quad (6)$$

So, Δn_{eff} measures, the absolute value within the *HE* and *EH* OAM modes. It must be larger than 10^{-4}.

The effective OAM mode area is symbolized by A_{eff} and can be evaluated through Eq. (7) (Jia et al. 2018).

$$A_{eff} = \frac{\left(\iint |E(x,y)|^2 dxdy\right)^2}{\iint |E(x,y)|^4 dxdy} \tag{7}$$

where $E(x, y)$ is an electric field allocation of the electromagnetic (EM) transverse field.

Numerical aperture (NA) can be calculated by Eq. (8) (Biswas et al. 2019).

$$\mathrm{NA} = \left[1 + \frac{\pi A_{eff}}{\lambda^2}\right]^{-\frac{1}{2}} \tag{8}$$

The nonlinear property of PCF is expressed through Eq. (9) and it is denoted by the γ (Jia et al. 2018).

$$\gamma = \frac{2\pi n_2}{\lambda A_{eff}} \tag{9}$$

where n_2 defines the nonlinear coefficient of fused silica and $n_2 = 2.6 \times 10^{-20}$ m^2/W.

Confinement loss (C_{loss}) can be evaluated by Eq. (10) (Xu et al. 2017).

$$C_{loss} = \frac{40\pi}{\ln(10)\lambda} Im\left(n_{eff}\right)(\mathrm{dB/m}) \tag{10}$$

where $Im\left(n_{eff}\right)$ is the unreal part of the refractive index of the OAM transmission mode and λ is the wavelength of the OAM mode.

3 Results and discussion

The proposed PCF supports 26 OAM modes with low confinement loss, flat dispersion, better nonlinearity, low numerical aperture and the refractive index difference greater than 10^{-4} between two adjacent OAM modes. Now, here is described the OAM properties such as an effective refractive index, dispersion, effective refractive index difference, effective mode area, numerical aperture, nonlinearity, and confinement loss with appropriate discussion, equation, and the necessary figure.

3.1 The effective refractive index of eigenmodes

The refractive index of fused silica is calculated by Eq. (1). Higher modes are obtained by decreasing the search around of the refractive index at a fixed wavelength.

Figure 3 shows the relationship between all selected OAM modes effective refractive index (n_{eff}) and wavelength within the range from 1.2 to 1.95 μm in the proposed PCF. The changing rate of the refractive index is downward with respect to the increment of wavelength. The effective refractive index is related to the dispersion. The flat dispersion is obtained for the small differences of the refractive index at any specific mode.

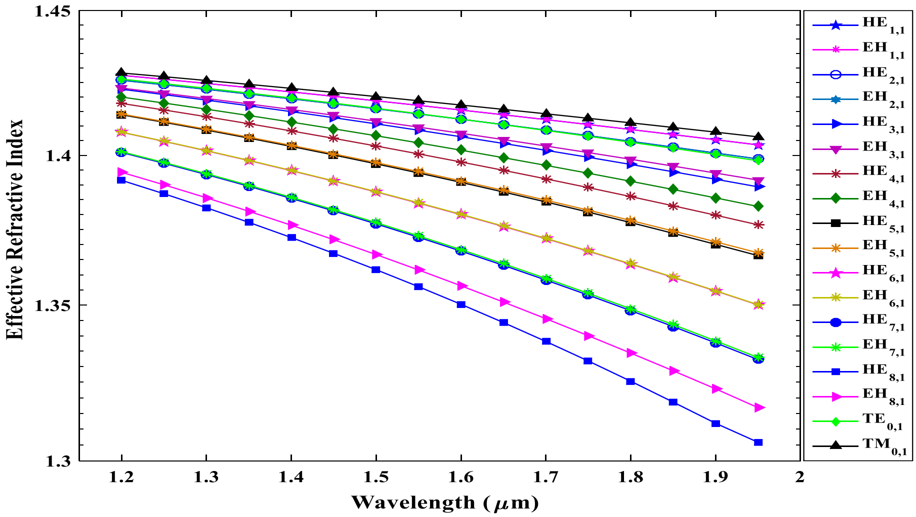

Fig. 3 The effective refractive index of different eigenmodes with respect to the wavelength

3.2 Dispersion

The dispersion parameter is one of the most important parameters of PCF. Dispersion is the expansion of the light pulse at transmitting time. It decreases the performance of an optical fiber. It contains material and waveguide dispersion (Zhang et al. 2018). Material dispersion has little effect on the total dispersion. So, the calculation is only for the waveguide dispersion.

The dispersion is inversely proportional to the wavelength. The $TM_{0,1}$, $TE_{0,1}$, $EH_{1,1}$, $HE_{1,1}$, $EH_{2,1}$, $HE_{2,1}$ and others OAM modes are exhibited in Fig. 4.

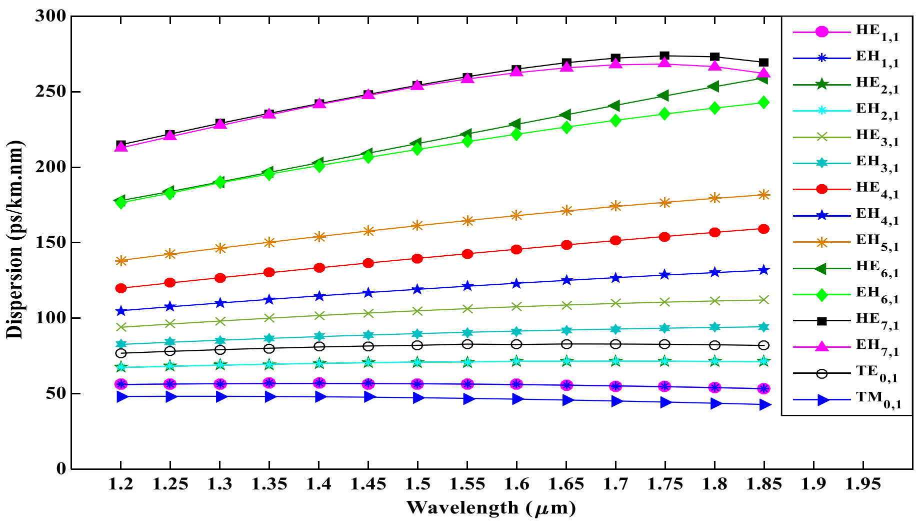

Fig. 4 Dispersion of different OAM modes with respect to the wavelength

The dispersion of $TE_{0,1}$, $EH_{1,1}$, $HE_{1,1}$, $EH_{2,1}$, $HE_{2,1}$, and $TM_{0,1}$ modes are nearly horizontal while other OAM modes show flat dispersion. The high dispersion is shown in $HE_{6,1}$ and $EH_{6,1}$ modes of the OAM. The proposed PCF shows the dispersion variation of different OAM modes. For example, the dispersion variation for the $TE_{0,1}$ mode is 5.1421 ps/km-nm, the $HE_{2,1}$ mode is 3.8684 ps/km-nm, the $HE_{3,1}$ mode is 18.0606 ps/km-nm, the $HE_{4,1}$ mode is 39.5561 ps/km-nm, the $HE_{6,1}$ mode is 64.8221 ps/km-nm, the $HE_{7,1}$ mode is 47.2286 ps/km-nm, the $EH_{2,1}$ mode is 3.8566 ps/km-nm, the $EH_{3,1}$ mode is 11.6646 ps/km-nm, the $EH_{4,1}$ mode is 26.7569 ps/km-nm, the $EH_{5,1}$ mode is 43.4371 ps/km-nm, the $EH_{6,1}$ mode is 81.6529 ps/km-nm, the $EH_{7,1}$ mode is 56.7001 ps/km-nm within the wavelength from 1.2 to 1.85 μm.

Especially, for the $TE_{0,1}$ and $HE_{2,1}$ mode, the variation of dispersion is much better than indicated values (Nandam and Shin 2018; Zhang et al. 2016; Yue et al. 2012).

The dispersion of the *HE* mode is larger than the *EH* mode. Because, the effective index of the *HE* mode is smaller than the *EH* mode in the same order of the OAM modes (Bai et al. 2018). In Fig. 4, the dispersion of $HE_{4,1}$ and the $EH_{4,1}$ mode is 142.6587 ps/km-nm and 121.1491 ps/km-nm respectively. So, the higher orders of the OAM modes have a higher dispersion.

The dispersion of the proposed PCF is improved by modifying the basic element of the PCF. The improvement of dispersion is also dependent on the small refractive index differences.

3.3 The effective refractive index difference of OAM modes

Figure 5 shows the relationship between the Δn_{eff} and wavelength. For the disparity, in Fig. 5, a blue straight line is used to indicate for the 10^{-4}. If differences of OAM modes (*HE* and *EH*) are not greater than 10^{-4}, then this mode will be coupled with one another, and also command to linearly polarized (LP). The Δn_{eff} *is* increased by increasing the wavelength. The higher order of the OAM modes will be highly effective refractive index differences (Δn_{eff}). The highest Δn_{eff} is 4.4302×10^{-2} at 1950 nm wavelength for $|HE_{8,1} - EH_{6,1}|$.

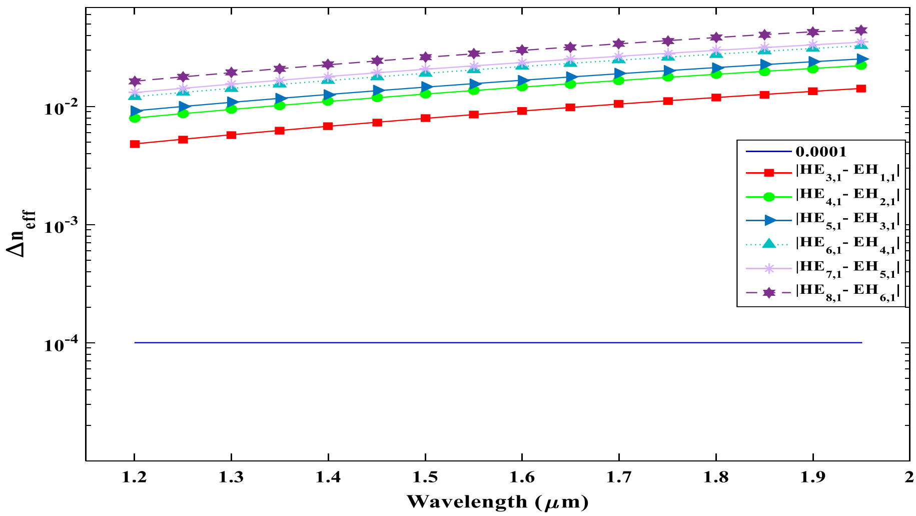

Fig. 5 Effective refractive index differences of different OAM modes with respect to the wavelength

Therefore, the PCF has the benefits of decrement of the OAM mode coupling as well as ensuring the robust transmission of OAM modes.

3.4 The effective mode area

The A_{eff} of the PCF has a significant response to the nonlinearity parameter. The effective area is increased by increasing with the wavelength. The effective area of different OAM modes is shown in Fig. 6.

Here, $TM_{0,1}$ and $TE_{0,1}$ achieves the lowest and the highest effective mode area respectively. The indicated part of Fig. 6 is the zoom view of the dashed shaped area that clarifies the effective mode area of different OAM modes. Low numerical aperture and nonlinearity are obtained for the flat effective area.

3.5 Numerical aperture (NA)

NA is acknowledged by the total amount of optical power. The higher values of NA have various applications in the optical field. Besides, the low values of NA provide depth of field (DOF).

From the Eq. (8), NA is dependent on the effective area and the wavelength. The NA is a unit less parameter. It is increased by increasing the wavelength as well as decreasing the effective area.

The indicated part of Fig. 7 is the zoom view of the dashed shaped area that clarifies the numerical aperture of different OAM modes.

The low numerical aperture of the proposed PCF is obtained for the random variations of the refractive index.

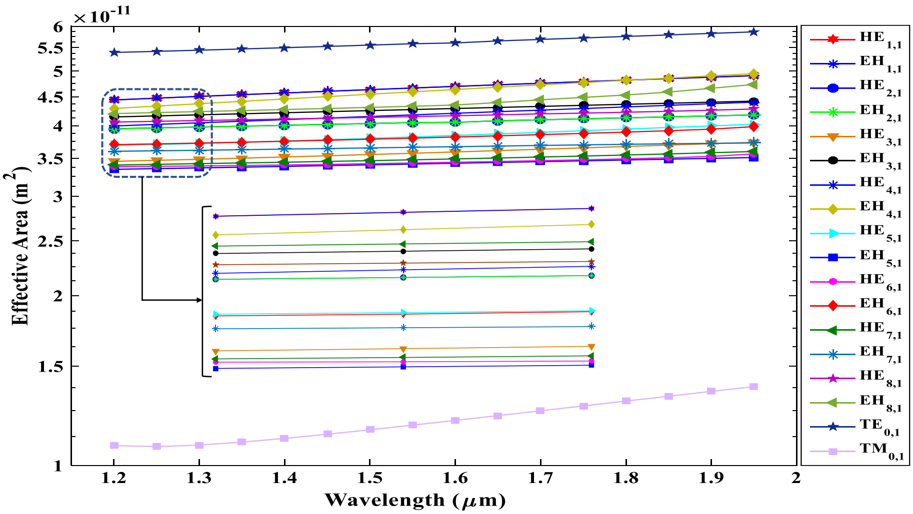

Fig. 6 The effective area of different OAM modes with respect to the wavelength

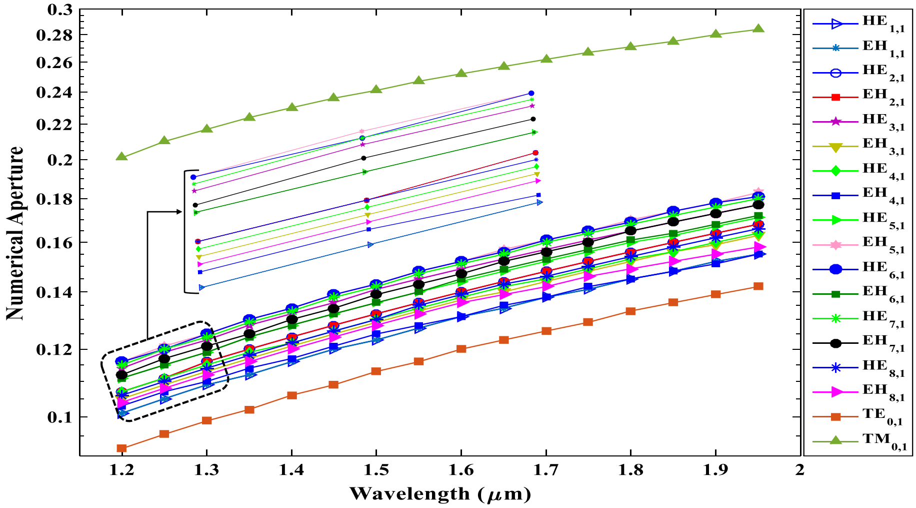

Fig. 7 The numerical aperture of different OAM modes with respect to the wavelength

3.6 Nonlinearity

Figure 8 displays the relationship between the nonlinearity and wavelength of all selected OAM modes. Nonlinearity is inversely proportional to the effective mode area and wavelength. In the proposed PCF, all selected OAM modes are low nonlinearity within the range from 1.2 to 1.95 μm. Especially, the nonlinearity of most OAM modes are below 4 W^{-1}/km and particularly, the lowest nonlinearity of $TE_{0,1}$ OAM mode is 1.58 W^{-1}/km at the wavelength 1.8 μm.

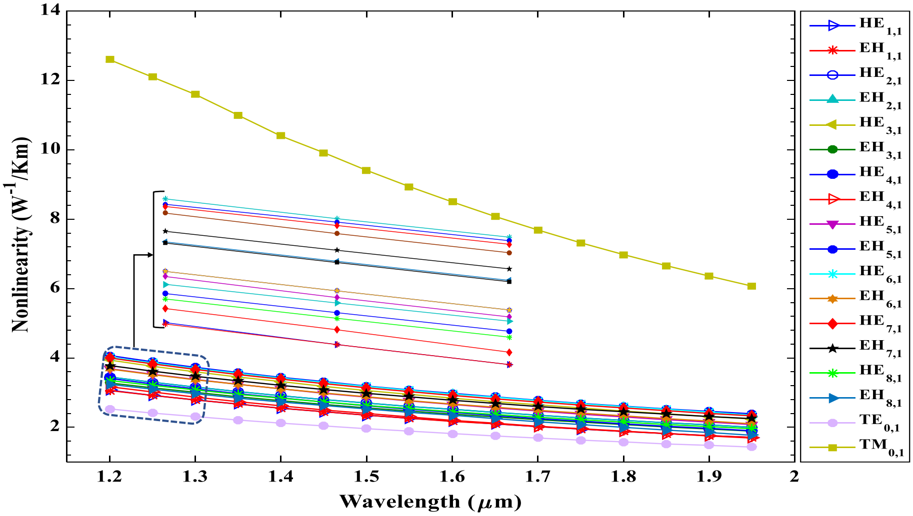

Fig. 8 Nonlinearity of different OAM modes with respect to the wavelength

The indicated part of Fig. 8 is the zoom view of the dashed shaped area that clarifies the nonlinearity of different OAM modes.

The proposed PCF is achieved lower nonlinearity. Because, lower nonlinearity is obtained for the large core (Hu et al. 2016).

3.7 Confinement loss (CL)

The confinement loss is caused by structural imperfection, micro bending, and intrinsic material absorption characteristics when light is transmitted over the PCF (Shi et al. 2019). The CL is determined for the different modes of the OAM. The CL for the $TM_{0,1}$, $TE_{0,1}$, $EH_{1,1}$, $HE_{1,1}$, $EH_{2,1}$, $HE_{2,1}$, and other modes are represented in the Fig. 9.

In the scenario of Fig. 9, the inconstancy of CL of all different OAM modes with respect to the wavelength does not display significant regularity. It is mainly adequate to the high probability of leakage to cladding for the larger wavelength. The indicated part of Fig. 9 is the zoom view of the dashed shaped area that clarifies the CL of different OAM modes from the wavelength 1.5 to 1.6 μm of step size 1 nm.

In this proposed PCF design, the average CL of the most OAM modes is varied between 4×10^{-10} and 5×10^{-6} dB/m with the wavelength from 1.2 to 1.95 μm. Such as, The $HE_{4,1}$ mode has the lowest confinement loss that is numerically 3.19×10^{-10} dB/m at wavelength 1.8 μm. In Fig. 9, the confinement loss of the $HE_{1,1}$ mode is 1.01×10^{-9} dB/m, the $EH_{1,1}$ mode is 6.62×10^{-9} dB/m, the $HE_{2,1}$ mode is 5×10^{-8} dB/m, the $EH_{2,1}$ mode is 3.46×10^{-7} dB/m, the $EH_{3,1}$ mode is 5.28×10^{-7} dB/m, the $HE_{4,1}$ mode is 3.22×10^{-7} dB/m, the $EH_{4,1}$ mode is 4.57×10^{-8} dB/m, the $EH_{6,1}$ mode is 3.39×10^{-7} dB/m, the $HE_{7,1}$ mode is 7.86×10^{-8} dB/m, the $EH_{7,1}$ mode is 6.15×10^{-9} dB/m and the $TE_{0,1}$ mode is 1.5×10^{-7} dB/m at the wavelength of 1.45 μm.

The CL is destructive for the optical communication system. The CL is generated for structural imperfection and internal absorption. The CL of the proposed PCF is decreased

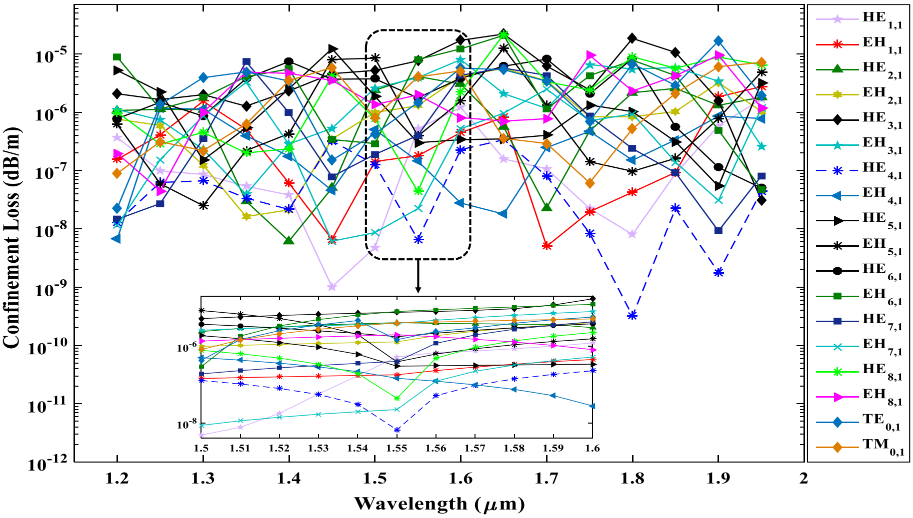

Fig. 9 Confinement loss of different OAM modes with respect to the wavelength

Table 1 The comparison chart of dispersion variations for TE, HE modes and confinement loss of the proposed article and the recent published articles

References (prior PCFs)	Operating wavelength for CL (nm)	Dispersion variation of $TE_{0,1}$ (ps/km-nm)	Dispersion variation of $HE_{2,1}$ (ps/km-nm)	Confinement loss (dB/m)
Nandam and Shin (2018)	1550	10.35	12.1	5.0951×10^{-3}
Zhang et al. (2017b)	1550	–	–	9.52×10^{-9}
Zhang et al. (2016)	1550	<46.38	–	3.434×10^{-9}
Yue et al. (2012)	> 2000	< 60	–	$<3\times10^{-2}$
This work	1800	5.1421	3.8684	3.19×10^{-10}

for periodic cladding. For all OAM modes confinement loss does not show the regularity. It is caused for a greater chance of leakage to the cladding (fused silica) for higher wavelength.

The comparison of confinement loss and dispersion variation of OAM modes with some previous article of OAM based PCF is shown in Table 1.

By comparing with some OAM modes PCF parameters that are previously reported and it can be investigated that our proposed PCF gives much better optical characteristics than other OAM based PCF articles.

4 Conclusion

In this article, a novel chain-shape PCF design is proposed with low confinement loss, flat dispersion, better nonlinearity and high refractive index differences between the wide bandwidth the range of 750 nm (from 1200 to 1950 nm). The proposed fiber parameters are numerically calculated by applying FEM and PML as a boundary condition. The design can support up to 26 OAM modes. The numerical exploration shows that the effective refractive index differences of all selected OAM modes are above than 10^{-4}. The maximum Δn_{eff} is 4.4302×10^{-2} at 1950 nm wavelength for $HE_{8,1}$ to $EH_{6,1}$ mode. The low confinement loss is 3.19×10^{-10} dB/m at optical wavelength 1800 nm. The dispersion variation for the $HE_{2,1}$ mode is 3.8684 ps/km nm and 5.1421 ps/km nm for $TE_{0,1}$ mode. So, the proposed PCF will be a strong candidate in stable and high capacity transmissions, encoding and MDM applications.

Acknowledgements This manuscript has not been published yet and not even under consideration for publication elsewhere. The authors are grateful who have participated in this research work.

Funding There is no funding for this work.

Compliance with ethical standards

Conflict of interest All the authors have read the manuscript and approved this for submission as well as no competing interests.

References

Allen, L., Beijersbergen, M.W., Spreeuw, R.J.C., Woerdman, J.P.: Orbital angular momentum of light and the transformation of Laguerre-Gaussian laser modes. Phys. Rev. A **45**(11), 8185–8189 (1992)

Bai, X., Chen, H., Yang, H.: Design of a circular photonic crystal fiber with square air-holes for orbital angular momentum modes transmission. Optik **158**, 1266–1274 (2018)

Biswas, B., Ahmed, K., Paul, B.K., Khalek, M.A., Uddin, M.S.: Numerical evaluation of the performance of different materials in nonlinear optical applications. Results Phys. **13**, 102184 (2019)

Brunet, C., Vaity, P., Messaddeq, Y., LaRochelle, S., Rusch, L.A.: Design, fabrication and validation of an OAM fiber supporting 36 states. Opt. Express **22**(21), 26117–26127 (2014)

Chen, C., Zhou, G., Zhou, G., Xu, M., Hou, Z., Xia, C., Yuan, J.: A multi-orbital-angular-momentum multi-ring micro-structured fiber with ultra-high-density and low-level crosstalk. Opt. Commun. **368**, 27–33 (2016)

Fang, L., Wang, J.: Flexible generation/conversion/exchange of fiber-guided orbital angular momentum modes using helical gratings. Opt. Lett. **40**(17), 4010–4013 (2015)

Heng, X., Gan, J., Zhang, Z., Qian, Q., Xu, S., Yang, Z.: Controlled generation of different orbital angular momentum states in a hybrid optical fiber. Opt. Commun. **402**, 668–671 (2017)

Hu, Z.A., Huang, Y.Q., Luo, A.P., Cui, H., Luo, Z.C., Xu, W.C.: Photonic crystal fiber for supporting 26 orbital angular momentum modes. Opt. Express **24**(15), 17285–17291 (2016)

Huang, H., Xie, G., Yan, Y., Ahmed, N., Ren, Y., Yue, Y., Rogawski, D., Willner, M.J., Erkmen, B.I., Birnbaum, K.M., Dolinar, S.J.: 100 Tbit/s free-space data link enabled by three-dimensional multiplexing of orbital angular momentum, polarization, and wavelength. Opt. Lett. **39**(2), 197–200 (2014)

Jia, C., Jia, H., Wang, N., Chai, J., Xu, X., Lei, Y., Liu, G., Peng, Y., Xie, J.: Theoretical analysis of a 750-nm bandwidth hollow-core ring photonic crystal fiber with a graded structure for transporting 38 orbital angular momentum modes. IEEE Access **6**, 20291–20297 (2018)

Jiao, X., Zhang, H., Zhang, X., Li, H., Wei, J., Wang, Z., Xi, L., Zhang, W., Tang, X.: Performance of circular photonic crystal fiber transmitting orbital angular momentum modes under macro-bending. J. Opt. **21**(6), 065703 (2019)

Lei, Y., Xu, X., Wang, N., Jia, H.: Numerical analysis of a photonic crystal fiber for supporting 76 orbital angular momentum modes. J. Opt. **20**(10), 105701 (2018)

Li, H., Ren, G., Lian, Y., Zhu, B., Tang, M., Zhao, Y., Jian, S.: Broadband orbital angular momentum transmission using a hollow-core photonic bandgap fiber. Opt. Lett. **41**(15), 3591–3594 (2016)

Li, H., Zhang, H., Zhang, X., Zhang, Z., Xi, L., Tang, X., Zhang, W., Zhang, X.: Design tool for circular photonic crystal fibers supporting orbital angular momentum modes. Appl. Opt. **57**(10), 2474–2481 (2018)

Li, C., Yan, B., Liu, J.: Refractive index sensing characteristics in a D-shaped photonic quasi-crystal fiber sensor based on surface plasmon resonance. JOSA A **36**(10), 1663–1668 (2019)

Liu, J., Fan, Z.: Size limits for focusing of two-dimensional photonic quasicrystal lenses. IEEE Photonics Technol. Lett. **30**(11), 1001–1004 (2018)

Liu, E., Yan, B., Tan, W., Xie, J., Ge, R., Liu, J.: Guiding characteristics of sunflower-type fiber. Superlattices Microstruct. **115**, 123–129 (2018)

Liu, E., Tan, W., Yan, B., Xie, J., Ge, R., Liu, J.: Robust transmission of orbital angular momentum mode based on a dual-cladding photonic quasi-crystal fiber. J. Phys. D Appl. Phys. **52**(32), 325110 (2019a)

Liu, E., Liang, S., Liu, J.: Double-cladding structure dependence of guiding characteristics in six-fold symmetric photonic quasi-crystal fiber. Superlattices Microstruct. **130**, 61–67 (2019b)

Liu, Q., Yan, B., Liu, J.: U-shaped photonic quasi-crystal fiber sensor with high sensitivity based on surface plasmon resonance. Appl. Phys. Express **12**(5), 052014 (2019c)

Liu, Q., Sun, J., Sun, Y., Liu, W., Wang, F., Yang, L., Liu, C., Liu, Q., Li, Q., Ren, Z., Sun, T.: Surface plasmon resonance sensor based on eccentric core photonic quasi-crystal fiber with indium tin oxide. Appl. Opt. **58**(25), 6848–6853 (2019d)

Monfared, Y.E.: Transient dynamics of stimulated Raman scattering in gas-filled hollow-core photonic crystal fibers. Adv. Mater. Sci. Eng. **2018**, 8951495 (2018)

Monfared, Y.E., Mojtahedinia, A., Javan, A.M., Kashani, A.M.: Highly nonlinear enhanced-core photonic crystal fiber with low dispersion for wavelength conversion based on four-wave mixing. Front. Optoelectron. **6**(3), 297–302 (2013)

Nandam, A., Shin, W.: Spiral photonic crystal fiber structure for supporting orbital angular momentum modes. Optik **169**, 361–367 (2018)

Padgett, M., Bowman, R.: Tweezers with a twist. Nat. Photonics **5**(6), 343–348 (2011)

Pakarzadeh, H., Sharif, V.: Control of orbital angular momentum of light in optofluidic infiltrated circular photonic crystal fibers. Opt. Commun. **438**, 18–24 (2019)

Ren, J., Sun, X., Wang, S.: A low threshold nanocavity in a two-dimensional 12-fold photonic quasicrystal. Opt. Laser Technol. **101**, 42–48 (2018)
Richardson, D.J., Fini, J.M., Nelson, L.E.: Space-division multiplexing in optical fibres. Nat. Photonics **7**(5), 354–362 (2013)
Shi, A., Ge, R., Liu, J.: Refractive index sensor based on photonic quasi-crystal with concentric ring microcavity. Superlattices Microstruct. **133**, 106198 (2019)
Tamburini, F., Anzolin, G., Umbriaco, G., Bianchini, A., Barbieri, C.: Overcoming the Rayleigh criterion limit with optical vortices. Phys. Rev. Lett. **97**(16), 163903 (2006)
Tang, Y., Deng, J., Li, K.F., Jin, M., Ng, J., Li, G.: Quasicrystal photonic metasurfaces for radiation controlling of second harmonic generation. Adv. Mater. **31**(23), 1901188 (2019)
Wang, J., Yang, J.Y., Fazal, I.M., Ahmed, N., Yan, Y., Huang, H., Ren, Y., Yue, Y., Dolinar, S., Tur, M., Willner, A.E.: Terabit free-space data transmission employing orbital angular momentum multiplexing. Nat. Photonics **6**(7), 488–496 (2012)
Wang, N., Xie, J.L., Jia, H.Z., Chen, M.M.: A low confinement loss double-photonic crystal fibre over 850 nm bandwidth with 26 orbital angular momentum modes transmission. J. Mod. Opt. **65**(18), 2060–2064 (2018)
Wong, G.K.L., Kang, M.S., Lee, H.W., Biancalana, F., Conti, C., Weiss, T., Russell, P.S.J.: Excitation of orbital angular momentum resonances in helically twisted photonic crystal fiber. Science **337**(6093), 446–449 (2012)
Xu, X., Jia, H., Lei, Y., Jia, C., Liu, G., Chai, J., Peng, Y., Xie, J.: Theoretical proposal of a low-loss widebandwidth silicon photonic crystal fiber for supporting 30 orbital angular momentum modes. PLoS ONE **12**(12), e0189660 (2017)
Xu, M., Zhou, G., Chen, C., Zhou, G., Sheng, Z., Hou, Z., Xia, C.: A novel micro-structured fiber for OAM mode and LP mode simultaneous transmission. J. Opt. **47**(4), 428–436 (2018)
Yan, B., Wang, A., Liu, E., Tan, W., Xie, J., Ge, R., Liu, J.: Polarization filtering in the visible wavelength range using surface plasmon resonance and a sunflower-type photonic quasi-crystal fiber. J. Phys. D Appl. Phys. **51**(15), 155105 (2018)
Yue, Y., Zhang, L., Yan, Y., Ahmed, N., Yang, J.Y., Huang, H., Ren, Y., Dolinar, S., Tur, M., Willner, A.E.: Octave-spanning supercontinuum generation of vortices in an As 2 S 3 ring photonic crystal fiber. Opt. Lett. **37**(11), 1889–1891 (2012)
Zhang, H., Zhang, W., Xi, L., Tang, X., Tian, W., Zhang, X., Zhang, X.: Design of a circular photonic crystal fiber supporting OAM modes. In: Asia Communications and Photonics Conference, pp. ASu2A-54. Optical Society of America (2015)
Zhang, H., Zhang, W., Xi, L., Tang, X., Zhang, X., Zhang, X.: A new type circular photonic crystal fiber for orbital angular momentum mode transmission. IEEE Photonics Technol. Lett. **28**(13), 1426–1429 (2016)
Zhang, H., Zhang, X., Li, H., Deng, Y., Xi, L., Tang, X., Zhang, W.: The orbital angular momentum modes supporting fibers based on the photonic crystal fiber structure. Crystals **7**(10), 286 (2017a)
Zhang, H., Zhang, X., Li, H., Deng, Y., Zhang, X., Xi, L., Tang, X., Zhang, W.: A design strategy of the circular photonic crystal fiber supporting good quality orbital angular momentum mode transmission. Opt. Commun. **397**, 59–66 (2017b)
Zhang, L., Zhang, K., Peng, J., Deng, J., Yang, Y., Ma, J.: Circular photonic crystal fiber supporting 110 OAM modes. Opt. Commun. **429**, 189–193 (2018)
Zhu, Y., Zou, K., Zheng, Z., Zhang, F.: 1 $\lambda \times 1.44$ Tb/s free-space IM-DD transmission employing OAM multiplexing and PDM. Opt. Express **24**(4), 3967–3980 (2016)